Nutrient chemotaxis suppression of a diffusive instability in bacterial colony dynamics

Scott Arouh and Herbert Levine
Physics Department, University of California, San Diego, 9500 Gilman Drive, La Jolla, California 92093-0319
(Received 17 November 1999; revised manuscript received 20 January 2000)

Bacteria grown on a semisolid agar surface have been observed to form branching patterns as the colony envelope propagates outward. The fundamental cause of this instability relates to the need for limited nutrient to diffuse towards the colony. Here, we investigate the effect on this instability of allowing the bacteria to move chemotactically in response to the nutrient gradient. Our results show that this additional effect has a tendency to suppress the instability. Our calculations are done within the context of a simple ''cutoff'' model of colony dynamics, but presumably remain valid for more complex and hence more realistic approaches.

PACS number(s): 87.10.+e

When bacteria are grown on a semisolid agar surface, their resultant colonies have been observed to form a variety of spatial patterns, depending on bacterial species and environmental conditions (nutrient levels, agar hardness, temperature). These include spots and rings in *Salmonella typhimurium* [1] and *Escherichia coli* [2]; branched colonies, chiral structures, and vortices in *Bacillus subtilis* and related species [3–6]; and terraced rings in *Proteus mirabilis* [7], *Vibrio parahaemolyticus* [8], and *Bacillus subtilis* [9]. Here, we focus on one of the patterns of *Bacillus subtilis* and *Paenibacillus dendritiformis* [10], in which an initially round two-dimensional (2D) colony develops a disorderd, tip-splitting structure as it expands.

It is clear that the basic mechanism underlying this pattern formation process is a diffusive, Mullins-Sekerka instability. Systems with this instability often generate patterns that are characterized by fingerlike projections growing out of the propagating front. A variety of systems have been observed to exhibit these diffusive instabilities; examples include 2D electrochemical deposition between a center and a surrounding electrode and 2D Hele-Shaw cells of air injection into a glycerol layer [11–13]. It has therefore been important to generate models of the bacterial system that exhibit this instability. Surprisingly, the simplest two-component reaction-diffusion system that one might use, namely, the diffusive Fisher equation [10], does not suffice for this purpose. One must therefore include either a metastable reaction term [14], a cutoff due to finite particle number [15], or nonlinear bacterial diffusion [16,17]. These models are compared and contrasted in Ref. [10].

Ben-Jacob and co-workers have suggested [18,19] that several aspects of the observed patterns can only be understood if one includes the chemotactic capabilities of the bacteria. Motivated by this, we study here the effect that nutrient chemotaxis, namely, bacterial swimming towards food, has on the diffusive instability. We will show that inclusion of this term tends to suppress the instability. Our calculations are done with the Kessler-Levine cutoff approach [15] briefly reviewed below, but should apply independently of the precise diffusive model.

Our starting point is the Kessler-Levine equations

$$\partial_t u = D\nabla^2 u + \gamma \eta u \Theta(u-\epsilon),$$
$$\partial_t \eta = \nabla^2 \eta - \eta u \Theta(u-\epsilon), \tag{1}$$

where $\Theta(x)$ is the Heaviside step function (1 if $x>0$, 0 otherwise). In this model, bacteria (with density u) swim around (diffuse), eat nutrients (with concentration η, which also diffuses), and reproduce. The cutoff in the reaction at small bacterial density arises via consideration of the discreteness of individual bacteria and is responsible for the existence of a diffusive instability. This latter fact, that there is a critical diffusion constant that goes to zero in the limit $\epsilon \to 0$ (the model without a cutoff), was explained at length in Ref. [15]. Roughly, the effective width of the u interface, defined as the distance one must go to reach the cutoff [starting from densities of O(1)], scales as $(-D \ln \epsilon)$; this must be smaller than the η-field diffusion length $(1/v)$ for there to be an instability. Since the velocity goes to a finite limit as $\epsilon \to 0$, this predicts $D_{crit} \sim -1/\ln \epsilon$, in agreement with the calculated results.

To include nutrient chemotaxis, we modify this model to

$$\partial_t u = D\nabla^2 u - \nabla[\xi(u,\eta)\nabla\eta] + \gamma \eta u \Theta(u-\epsilon),$$
$$\partial_t \eta = \nabla^2 \eta - \eta u \Theta(u-\epsilon). \tag{2}$$

Here we have introduced a new bacterial flux term proportional to nutrient density gradient $\nabla\eta$, with a coefficient dependent on bacterial density u and nutrient density η. A typical choice for ξ is the receptor law,

$$\xi(u,\eta) = \xi_0 \frac{K}{(K+\eta)^2} u, \tag{3}$$

where K is the receptor dissociation constant of the receptor; this arises from using the gradient of the number of bound receptors as the relevant biological signal.

The basic idea is to find uniformly propagating front solutions for this system and then find the resulting stability spectrum. The calculation proceeds as follows. First, we obtain asymptotic expressions in the two cases $x \to -\infty$, $x \to +\infty$, for the steady-state profiles. Given these expressions,

we can numerically integrate these unperturbed equations inward from each of the boundaries toward a central matching point. We choose this point to be the place where the bacterial density equals ϵ and denote it as $x=x_\epsilon$. Demanding continuity of u^0, η^0 and their first derivatives fixes the free parameters in the aforementioned asymptotic solution. With the unperturbed solutions in hand, we can numerically integrate the equations for the perturbation solutions ψ_u, ψ_η, again starting from the boundaries and matching in the middle. This system is solvable only if the assumed growth rate ω is properly fixed. Thus, we can determine the growth rate ω as a function of perturbation wave number q, thereby finding the stability spectrum.

We first obtain the values of the unperturbed solutions and their derivatives at the right boundary ($x\to+\infty$). The governing equation in the frame moving with velocity v becomes

$$0=vu'+\gamma\eta u\Theta(u-\epsilon)+Du''-(\xi_u u'\eta'+\xi_\eta\eta'^2+\xi\eta''),$$

$$0=v\eta'+\eta''-\gamma\eta u\Theta(u-\epsilon), \tag{4}$$

where $\xi_u=\partial_u\xi(u,\eta)$, $\xi_\eta=\partial_\eta\xi(u,\eta)$, and $\xi(u,\eta)$ is as given in Eq. 3. In the $x\to+\infty$ limit, imposing $u\to0$ and $\eta\to1$ reduces Eq. 4 to

$$0=vu'+Du'',$$

$$0=v\eta'+\eta'', \tag{5}$$

with solutions

$$u(x)=0+B_1e^{-(v/D)(x-x_\epsilon)},$$

$$\eta(x)=1-\delta_1e^{-v(x-x_\epsilon)}. \tag{6}$$

The unspecified parameters B_1 and δ_1 are to be determined later from the matching conditions. These conditions enable us to integrate Eq. 4 and find the values of the unperturbed solutions and their derivatives at the matching point x_ϵ. A similar analysis at large negative x leads to

$$u(x)=1+\delta_2-\delta_3e^{kx},$$

$$\eta(x)=B_2e^{kx}, \tag{7}$$

where

$$B_2=\frac{\delta_3k(v+Dk)}{\gamma(1+\delta_2)-\xi(u=1+\delta_2,\eta=0)k^2},$$

$$k=-\frac{v}{2}+\sqrt{\left(\frac{v}{2}\right)^2+(1+\delta_2)}. \tag{8}$$

Then, the basic equation can be integrated forward to the matching point. Furthermore, we choose the origin of our coordinates such that $x_\epsilon=0$. Four continuity conditions plus $u(0)=\epsilon$ yield five conditions for the five unknowns $(v,\delta_1,\delta_2,\delta_3,B_1)$. Due to an overall conservation law, $1+\delta_2=\gamma$, and this serves as a test of the numerical root-finding procedure.

Next, we perform a similar analysis for an assumed perturbation $\psi_u(x)$, $\psi_\eta(x)$, where

$$u(x,y,t)=u^0(x-vt)+\psi_u(x-vt)e^{iqy+\omega t},$$

$$\eta(x,y,t)=\eta^0(x-vt)+\psi_\eta(x-vt)e^{iqy+\omega t}. \tag{9}$$

The linearized equations for the perturbation amplitudes are

$$\begin{aligned}(\omega+Dq^2)\psi_u=&v\psi_u'+D\psi_u''+\gamma(\eta^0\psi_u+u^0\psi_\eta)\Theta(u^0-\epsilon)\\&-\psi_u(\xi^0_{uu}\eta^{0\prime}u^{0\prime}+\xi^0_u\eta^{0\prime\prime}+\xi^0_{u\eta}\eta^{0\prime2})-\psi_\eta\\&\times(-\xi^0q^2+\xi^0_\eta\eta^{0\prime\prime}+\xi^0_{u\eta}u^{0\prime}\eta^{0\prime}+\xi^0_{\eta\eta}\eta^{0\prime2})\\&-\psi_u'\xi^0_u\eta^{0\prime}-\psi_\eta'(\xi^0_uu^{0\prime}+2\xi^0_\eta\eta^{0\prime})-\psi_\eta''\xi^0,\\(\omega+q^2)\psi_\eta=&v\psi_\eta'+\psi_\eta''-(\eta^0\psi_u+u^0\psi_\eta)\Theta(u^0-\epsilon).\end{aligned} \tag{10}$$

The first line on the right-hand side of the ψ_u equation and the entire ψ_η equation are the same as those used in the Kessler-Levine analysis; the remaining lines consist of new terms associated with chemotaxis. We append to these equations the additional boundary conditions that $\psi_u(x)$ and $\psi_\eta(x)$ both $\to0$ as $x\to\pm\infty$.

We proceed to find the asymptotic form of the solutions to these equations. The calculations are straightforward but tedious. For large negative x, these linear equations have the solution

$$\psi_u(x)=A_1e^{k_1x}+A_2e^{k_2x},$$

$$\psi_\eta(x)=C_1e^{k_1x}, \tag{11}$$

with

$$k_1=-\frac{v}{2}+\sqrt{\left(\frac{v}{2}\right)^2+[\omega+q^2+(1+\delta_2)]},$$

$$k_2=-\frac{v}{2D}+\sqrt{\left(\frac{v}{2D}\right)^2+\frac{\omega+Dq^2}{D}},$$

$$C_1=A_1\frac{\omega-vk_1+D(q^2-k_1^2)}{\gamma(1+\delta_2)+\xi(u=1+\delta_2,\eta=0)(q^2-k_1^2)}. \tag{12}$$

For large positive x, we have

$$\psi_u=A_3e^{-k_3(x-x_\epsilon)},$$

$$\psi_\eta=A_4e^{-k_4(x-x_\epsilon)}. \tag{13}$$

where now

$$k_3=\frac{v}{2D}+\sqrt{\left(\frac{v}{2D}\right)^2+\frac{\omega+Dq^2}{D}},$$

$$k_4=\frac{v}{2}+\sqrt{\left(\frac{v}{2}\right)^2+(\omega+q^2)}. \tag{14}$$

Now that we have the values of the perturbation profiles ψ_u, ψ_η and their derivatives at both boundaries, we can numerically integrate from both boundaries to the matching point $x_\epsilon=0$ (again, defined to be the origin of our coordinates). Again, four continuity conditions (see below) plus an overall normalization condition yields five conditions for the

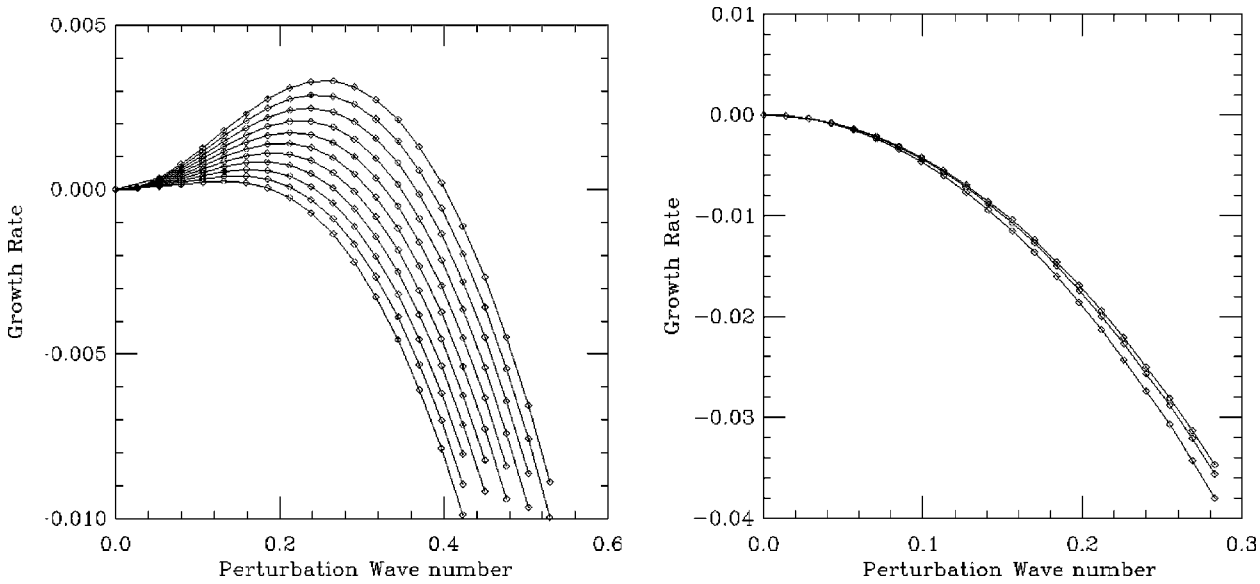

FIG. 1. Sample growth rate plots for perturbations to steady-state propagating front solutions. Plotted here are (*left*) a case with a cutoff-induced instability ($D=\frac{1}{7}$, $\epsilon=10^{-2}$, $\xi_0=0$) and (*right*) a stable case ($D=\frac{1}{2}$, $\epsilon=10^{-2}$, $\xi_0=0$). In each plot, the top curve is the nonchemotactic ($\xi_0=0$) case, and lower curves correspond to successively higher chemotactic strengths ξ_0. In the initially unstable case (left), these ξ_0 values range from 0.0 to 1.0 in steps of 0.1; in the initially stable case, only the values $\xi_0=0.0$, 0.3, 1.0 are plotted. Error bars for ω, based on the last trial values of free parameters before convergence was declared, are typically of the order of 10^{-5} or less and are not visible here.

five unknowns (A_1,A_2,A_3,A_4,ω). Hence, given a fixed wave vector q and an already determined unperturbed solution $u^0(x)$, $\eta^0(x)$ we can calculate the perturbed solution profile $\psi_u(x)$, $\psi_\eta(x)$ and the growth rate ω.

As mentioned above, when solving for the unperturbed solutions u^0, η^0, the conditions $x=x_\epsilon$ consist simply of continuity of the solutions and their derivatives, together with a condition fixing translation invariance. When solving for the perturbation profiles, however, although the solutions ψ_u, ψ_η themselves are continuous, their derivatives are not. The discontinuity at $x=x_\epsilon$ in ψ_u', ψ_η' arises from the $\Theta(u-\epsilon)$ cutoff in the model. We thus need to calculate the discontinuities $\Delta\psi_u'$, $\Delta\psi_\eta'$ across the interface, where

$$\Delta\psi'(x)\equiv\psi'(x^+)-\psi'(x^-). \tag{15}$$

Let us first compute this jump for the u field. Continuity of the derivatives of the full solution,

$$\Delta[u^{0\prime}(x)+\psi_u'(x)e^{i\vec{q}\cdot\vec{y}+\omega t}]=0 \tag{16}$$

and expansion of these values about the unperturbed front

$$u^{0\prime}(x_\epsilon+\delta x_\epsilon)=u^{0\prime}(x_\epsilon)+u^{0\prime\prime}(x_\epsilon)\,\delta x_\epsilon \tag{17}$$

gives this discontinuity in terms of the corresponding discontinuity in the second derivatives of the unperturbed solution $\Delta u^{0\prime\prime}(x_\epsilon)$ and the shift δx_ϵ in the position of the front due to the perturbation:

$$\Delta\psi_u'(x_\epsilon)e^{i\vec{q}\cdot\vec{y}+\omega t}=-\delta x_\epsilon\Delta u^{0\prime\prime}(x_\epsilon). \tag{18}$$

An analogous derivation leads to a similar expression for $\Delta\psi_\eta'(x_\epsilon)$. The interface shift can be found directly from the definition $u^0(x_\epsilon)\equiv\epsilon$ and $u(x_\epsilon+\delta x_\epsilon)\equiv\epsilon$ of the unperturbed and perturbed front, respectively; expanding, we get $u^0(x_\epsilon)+u^{0\prime}(x_\epsilon)\,\delta x_\epsilon+\psi_u(x_\epsilon)e^{i\vec{q}\cdot\vec{y}+\omega t}=\epsilon$ and hence

$$\delta x_\epsilon=-\frac{\psi_u(x_\epsilon)e^{i\vec{q}\cdot\vec{y}+\omega t}}{u^{0\prime}(x_\epsilon)}. \tag{19}$$

Finally, $\Delta u^{0\prime\prime}$, $\Delta\eta^{0\prime\prime}$ can be obtained directly from the original equations

$$\Delta u^{0\prime\prime}=\frac{[\gamma-\xi(x_\epsilon)]\eta^0(x_\epsilon)\epsilon}{D},$$

$$\Delta\eta^{0\prime\prime}=-\eta^0(x_\epsilon)\epsilon. \tag{20}$$

These expressions for $\Delta u^{0\prime\prime}$, $\Delta\eta^{0\prime\prime}$, and δx_ϵ yield the desired matching conditions for $\Delta\psi_u'$ and $\Delta\psi_\eta'$.

Using this method, we have calculated the growth rate ω versus perturbation wave number q for a representative selection of values of reaction threshold ϵ, bacterial to nutrient diffusivity ratio D, and chemotactic strength ξ_0. Specifically, we examined both cases for which a cutoff-induced instability already existed before chemotaxis was added ($D=\frac{1}{7}$, $\epsilon=10^{-2}$) and for which such an instability was absent ($D=\frac{1}{2}$, $\epsilon=10^{-2}$). In general, we used coefficients $\gamma=1$, $K=1$. Sample plots appear in Fig. 1. The fact that $\omega=0$ at zero wave vector is a consequence of translation invariance and serves as a test of the accuracy of our computations. Also, note in these plots that the uppermost curve corresponds to the case without chemotaxis, and these can be compared to earlier results [15].

As chemotaxis is turned on (ξ_0 increases from 0), we see that the growth rates become more negative (the curves get lower). This demonstrates nutrient chemotaxis repression of cutoff-induced Mullins-Sekerka instabilities in this system.

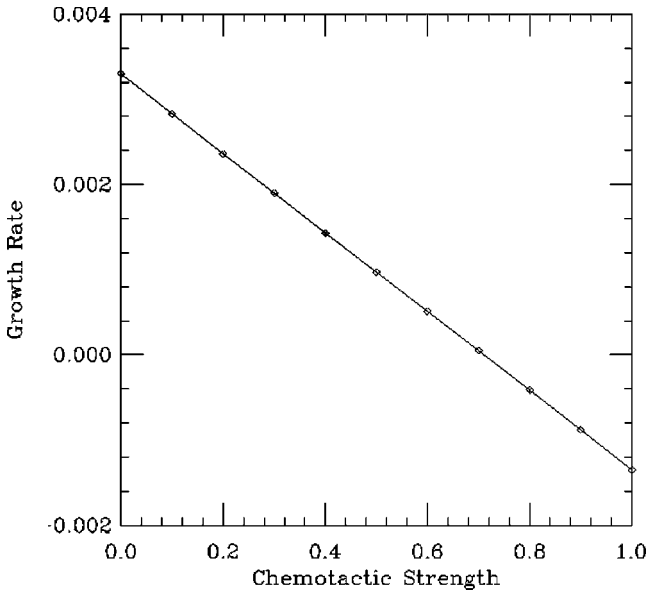

FIG. 2. Demonstration of linear repression of an initially unstable growth rate as nutrient chemotaxis is turned on. Plotted are the growth rate ω for the perturbation wave number $q=0.265$ (roughly the location where ω reaches its maximal value before chemotaxis is turned on) for values of ξ_0 for which ω vs q plots appear in Fig. 1. As in that figure, error bars are below the resolution of the figure.

The repression is further illustrated in Fig. 2, where it is seen to vary linearly with chemotactic strength ξ_0. Of course, this implies that a system with repulsive chemotaxis to an externally supplied field would exhibit an enhanced instability.

We verified that the saturation of chemoreceptors incorporated in the receptor law [Eq. (3)] was not crucial to the branching instability repression. In particular, we compared ω vs q plots with and without chemotaxis saturation. Our data (not shown) demonstrate that the nonlinearity in this law makes only a slight quantitative contribution to this suppression.

Why does chemotaxis suppress the onset of the instability, especially inasmuch as a naive analysis might lead one to argue that chemotaxis causes outwardly protruding parts of the colony to move faster as they feel higher gradients? This mechanism might well be important once the system exhibits well-developed fingers, and in fact it has been suggested [18] that nutrient chemotaxis is responsible for increasing the growth velocity without any concomitant change in colony structure. But, this is not the way in which chemotaxis affects the initial instability. Here, the chemotactic response gives rise to a increased velocity and hence a decrease in the nutrient field diffusion length. In particular, our results indicate that the nutrient profile becomes significantly sharper (data not shown) in the presence of chemotaxis. Since the instability requires that the interface be deformable on scales shorter than this diffusion length, this is now harder to accomplish and thus chemotaxis pushes the instability to lower D. Of course, the correctness of our calculations is independent of whether or not we can construct convincing arguments as to why the results should or should not have been expected.

Our analysis was carried out for one very specific model of the bacterial system. The real system is undoubtedly much more complicated and probably is best modeled by explicitly including an additional field for the fluid layer in which the bacteria move. So, one needs to verify that the suppression we have found will continue to hold for other models. Currently, we see no reason to suspect that the results would be different than those presented here; specifically, the aforementioned heuristic arguments regarding the changes in the nutrient profile applies in those models as well.

H.L. acknowledges the support of the US NSF under Grant No. DMR98-5735.

[1] D. Woodward, R. Tyson, M. Myerscough, J. Murray, E. Budrene, and H. Berg, Biophys. J. **68**, 2181 (1995).
[2] E. Budrene and H. Berg, Nature (London) **376**, 49 (1995).
[3] E. Ben-Jacob, H. Shmueli, O. Shochet, and A. Tenenbaum, Physica A **187**, 378 (1992).
[4] H. Fujikawa and M. Matsushita, J. Phys. Soc. Jpn. **58**, 3875 (1989).
[5] M. Matsushita and H. Fujikawa, Physica A **168**, 498 (1990).
[6] H. Fujikawa and M. Matsushita, J. Phys. Soc. Jpn. **60**, 88 (1991).
[7] O. Rauprich, M. Matsushita, C. Weijer, F. Siegert, S. Esipov, and J. Shapiro, J. Bacteriol. **178**, 6525 (1996).
[8] L. McCarter and M. Silverman, Mol. Microbiol. **4**, 1057 (1990).
[9] I. Ràfols, M.Sc. thesis, Chuo University, Japan, 1998.
[10] I. Golding, Y. Kozlovsky, I. Cohen, and E. Ben-Jacob, Physica A **260**, 510 (1998).
[11] E. Ben-Jacob and P. Garik, Nature (London) **343**, 523 (1990).
[12] M. Matsushita, M. Sano, Y. Hayakawa, H. Honjo, and Y. Sawada, Phys. Rev. Lett. **53**, 286 (1984).
[13] Y. Sawada, A. Dougherty, and J.P. Gollub, Phys. Rev. Lett. **56**, 1260 (1986).
[14] M. Matsushita, J. Wakita, H. Itoh, I. Rafols, T. Matsuyama, H. Sakaguchi, and M. Mimura, Physica A **249**, 517 (1998).
[15] D. Kessler and H. Levine, Nature (London) **394**, 556 (1998).
[16] S. Kitsunezaki, J. Phys. Soc. Jpn. **66**, 1554 (1997).
[17] K. Kawasaki, A. Mochizuki, T. Matsushita, T. Umeda, and N. Shigesada, J. Theor. Biol. **188**, 177 (1997).
[18] I. Cohen, A. Czirók, and E. Ben-Jacob, Physica A **233**, 678 (1996).
[19] E. Ben-Jacob, Contemp. Phys. **38**, 205 (1997).